Blade Trailing Edge Position Influencing Pump as Turbine (PAT) Pressure Field Under Part-load Conditions

Article *in* Renewable Energy · December 2018

DOI: 10.1016/j.renene.2018.12.077

CITATIONS
2

READS
140

7 authors, including:

Binama Maxime
Hohai University
13 PUBLICATIONS **30** CITATIONS
SEE PROFILE

Wen-Tao Su
Harbin Institute of Technology
25 PUBLICATIONS **66** CITATIONS
SEE PROFILE

Wei-Hua Cai
Harbin Institute of Technology
35 PUBLICATIONS **145** CITATIONS
SEE PROFILE

Xiao-Bin Li
Sun Yat-Sen University
59 PUBLICATIONS **321** CITATIONS
SEE PROFILE

Renewable Energy 136 (2019) 33–47

Contents lists available at ScienceDirect

Renewable Energy

journal homepage: www.elsevier.com/locate/renene

Blade trailing edge position influencing pump as turbine (PAT) pressure field under part-load conditions

Maxime Binama [a, b], Wen-Tao Su [a, *], Wei-Hua Cai [a], Xiao-Bin Li [c], Alexis Muhirwa [a], Biao Li [a, **], Emmanuel Bisengimana [d]

[a] School of Energy Science and Engineering, Harbin Institute of Technology, Harbin, 150001, China
[b] State Key Laboratory of Hydropower Equipment, Harbin Institute of Large Electric Machinery, Harbin, 150040, China
[c] Sino-French Institute of Nuclear Engineering and Technology, Sun Yat-Sen University, Zhuhai, 519082, China
[d] School of Mechanical Engineering, University of Rwanda, KN 73 St, Kigali, Rwanda

ARTICLE INFO

Article history:
Received 19 August 2018
Received in revised form
13 November 2018
Accepted 20 December 2018
Available online 21 December 2018

Keywords:
Pump as turbine
Pressure pulsations
Numerical analysis
Rotor-stator interaction

ABSTRACT

Small hydropower is the most preferred clean energy technology, especially in remote areas away from national electrical grid reach. Within these plants, Pump as Turbines (PATs) suffer from a very small range of optimum operating conditions, leading to a chronic vulnerability to off-design conditions and associated flow instability, as well as the resultant pressure pulsations. PAT impeller design presents a great opportunity to alter the flow dynamics within PAT flow zone, probably leading to PAT performance improvement. In this respect, the present study seeks to investigate the effect of blade trailing edge hub position on pressure field characteristics within a centrifugal PAT. Using the k-ε turbulence model, unsteady numerical simulations were carried on a three centrifugal PAT with different blade trailing edge hub positions, namely 15 mm, 20 mm, and 25 mm. The results showed that for PAT pressure pulsations distribution, the Rotor-stator Interaction (RSI) constitutes the main influencing factor, where the Blade Passing Frequency and its harmonics were the dominant frequencies, for the three models. Moreover; different PAT models exhibited different pressure pulsation characteristics. The Rh20 model exhibited the highest level of pressure pulsation amplitudes, while the lowest level of pressure pulsation was recorded with Rh15 model.

1. Introduction

In line with the recently adopted “go green” principle in all aspects of life where energy is, on a global scale, one of the most targeted fields; renewable energy sources exploitation is currently on the high rise like never before [1,2]. In this respect, hydropower constitutes the largest source of renewable energy, from which the extracted power can either be continuously supplied to national and local grids (large and small scale Hydros), or stored in huge amounts for power grid stabilization purposes (Pumped Storage plants) [3–6]. Due to different issues as daily recorded in these technologies, the power grid instability as inflicted by a high level penetration of different other renewable power sources (solar, wind) within the electrical grid and the cost-ineffectiveness of small scale hydroturbines for rural micro hydro-sites to say the least; special types of hydroturbines have been developed. This newly adopted technology (as compared to normal hydroturbine technology), consists of replacing a normal hydroturbine by a hydraulic pump impeller, resulting in a machine that can quite efficiently operate in both pumping and turbine modes. Depending on different aspects; machine size, operating circumstances and characteristics among others, these machines can either be classified as Pump as Turbines (PATs) or Reversible Pump Turbines (RPTs). PATs are normal pumps operated in reverse mode with no structural modification whatsoever and are generally installed at rural small scale hydropower sites with no reservoirs, mostly in hilly regions at farther locations from the national electrical grid reach [7–9]. On the other hand, RPTs are purposely made big-size centrifugal runners, with water flow control system in place (guide and stay vanes), and are mostly installed within Pumped Storage Plants (PSPs). RPTs, due to its flexibility in terms of quick and frequent operating mode switching ability, are known to have

* Corresponding author.
** Corresponding author.
E-mail addresses: suwentao@hit.edu.cn (W.-T. Su), biaoli@hit.edu.cn (B. Li).

https://doi.org/10.1016/j.renene.2018.12.077
0960-1481/

considerably improved the PSP operations, which in turn resulted in increased power supply operations safety and reliability. Nevertheless, for both RPTs and PATs, the rotor design plays a fundamental role in their efficient operations. For instance, for an RPT operating under off-design conditions, especially under low flow conditions, flow instabilities evolve at the runner inlet zones, accompanied by rotating stall cells development, which in turn successively block the runner flow channels [10–13], all leading to detrimental effects such as high pressure fluctuations and vibration [14], associated noise, and efficiency degradation. However, considering the fact that most of hydraulic losses have been found to take place in the runner, these flow instabilities and associated damages can be tamed through RPT runner design modifications, as demonstrated through different studies; Yin et al. [15], Olimstad et al. [16], Zhu et al. [17], Tao et al. [18] and Kerschberger et al. [19] among others. More about the RPT flow instabilities have been explained in details through different review articles as published by Zhang at al. [20], Binama at al. [2], and Zuo at al. [21,22].

In the same respect, efficient PAT operations, for both conventional and reverse modes, have been found to mainly depend on the impeller geometric design parameters. When under conventional operating conditions, which simply means normal pump operating conditions, the impeller plays a fundamental role in tackling different issues, cavitation and flow instability among others. Luo et al. [23] modified the pump impeller inlet design through both the extension of blade leading edge (BLE) and blade inlet angle, leading to improved pump operations. Moreover large incidence angle at extended blade LE were found to considerably improve the pump cavitation performance. In the same respect, through the use of a radial basis Function, Zhang et al. [24], trying to tackle the cavitation problem, extended the impeller blade LE forward along the shroud, resulting in a considerable pump cavitation performance improvement. The tip clearance between the runner blade tip and shroud can lead to tip flow leakage which in turn results in the emergence of different complex flow structures at the same zones and vicinities. Liu et al. [25,26] recorded the pump efficiency gradual degradation with an increase in blade tip clearance, where tip leakage vortex eventually got enhanced. The later was also found to be highly sensitive to the pump flow discharge. The same phenomenon was explored by Yue Hao and Lei Tan [27], where not only the influence of the tip clearance size was investigated but also its symmetry or asymmetry effect to the pump cavitation performance. The tip clearance asymmetric feature exhibited worse pump cavitation performance where the corresponding radial force fluctuations were 7 times the ones with a symmetric design. For pumps pumping viscous fluids, the friction losses on the rotor are much higher than the normal water pump case, which in turn affects their performance. Shojaeefar et al. [28], in the attempt to improve the efficiency for such a pump, investigated different sets of flow passage width-impeller outlet angle measures, where among the obtained results, the increase of impeller flow width was found to improve the pump efficiency. The effect of a prewhirl regulation system on pump performance characteristics, was explored by Liu et al. [29], where different prewhirl setups have shown a big impact on pump flow unsteadiness development mechanism. In addition to the above, more impeller design modifications were investigated; impeller trimming [30], impeller meridional flow passage modification [31], blade outlet design and blade wrap angle [32,33] to say the least, where the results were in some cases quite satisfying.

When under reverse operating conditions, PATs get to their BEP at comparatively higher Heads and flows, where the incurred flow structures as well as the associated hydraulic losses are different from the conventional operating conditions. Note that PAT's adoption at the expense of formerly used small scale hydraulic turbines for rural hydro-sites is more connected to its cost-effectiveness than anything else. Its intolerance to off-design operating conditions undermines its efficient operations. Therefore the improvement of PAT operational efficiency is still an open field for future research endeavors. One of the most important steps towards PAT efficiency improvement would be the identification of incurred losses and the mechanism by which they occur. As noted by Chapallaz et al. [34], the link between PAT reverse and conventional modes and associated flow characteristics for different sizes and types, can hardly be found. However, the incurred losses may be anything among friction losses, shock losses, and leakage losses. In line with this, Yang at al. [35] and Rawal and Kshirsagar [36] blamed the PAT runner to be the base of hydraulic losses occurrence. Lueneburg and Nelson [37] on the other hand, recommended runner inlet shock losses reduction to improve the machine overall efficiency. Therefore, PAT runner design features still constitute the main point of focus from which PAT incurred losses may be if not eliminated then reduced to a certain extent. To this end, different studies aiming at PAT performance improvements have been carried out. Doshi et al. [38] and Singh and Nestmann [39] have conducted almost similar studies about impeller inlet edges rounding. Considering the fact that the PAT inlet design significantly influences the local velocity triangle characteristics and hence the rotational momentum as transferred to the impeller, they decided to smoothen both the blade leading edge and the impeller hub and shroud inlet edges into a “bullet head”-like shape (edge rounding). The performed modifications were found to decrease the flow wakes at the runner inlet, thus improving the machine's overall efficiency. However, it was also pointed out that the backwardness on PAT impeller blades still causes more wakes than what the rounding technic can handle. Note that the point made in this study as one of recommended future research orientations about knowing whether the performed modifications would work well even with the conventional operating mode, had been addressed by Gao et al. [40] a year before (2016). In the same respect, Wang et al. [41], after noticing that the backward-curved blades of normal centrifugal pumps don't just fit their reverse mode operations, which in turn contributes to increased losses within the impeller, decided to design a new impeller with forward-curved blades, where the effect of different associated blade inlet angles on PAT reverse operations was investigated. The BEP flow rate was found to increase with the blade inlet angle, where the selection of the most suitable blade inlet angle among the four investigated values, actually led to considerably reduced energy losses within the impeller, with a significant efficiency increase from 59.98% to 67.91% as compared to the backward-curved blades design. In a study as carried out by Yang et al. [42], The addition of splitter blades to the original PAT impeller design showed great performance improvement in terms of efficiency, where a considerable reduction of pressure pulsations throughout all the investigated PAT components was achieved. Barrio et Al. [43] analyzed the pump blade-volute interactions through impeller trimming method, where the impeller-tongue gap reduction resulted in blade dynamic loads increment. Yang et al. [44] investigated the same parameter, under reverse operating mode. From the carried out PAT's unsteady pressure field analysis results, with the rotor-stator gap increase, the amplitude of high frequency unsteady pressure pulsation within the volute caused by the rotor-stator interaction was decreased, while the amplitude of the low frequency unsteady pressure within the impeller remained unchanged. In addition to the above, more PAT performance improvement attempts through impeller design modification such as the blade camber line modification [45], impeller trimming [46], impeller diameter modification [47], blade thickness variation [48], and blades number variation [49] to say

the least, have been made.

The here above presented impeller design modifications have positively impacted PAT operational characteristics and incurred flow dynamics, mainly by reducing the incurred hydraulic losses, which in turn led to more efficient PAT operations. However, there is still a widely open research space in this field, as despite the already spent efforts, PAT's off-design poor performance still constitutes a big hindrance to the PAT technology. In the literature, an even bigger number of already conducted investigations have been more focused on PAT performance prediction [50–52], and the progress is of a substantial value so far. However, little has been done on CFD prediction of unsteady pressure field characteristics, which in turn are closely related to PAT flow dynamics, thus having a direct impact on its performance. Note that these machines are for most of times run under off-design conditions, thus being victims to different flow instabilities occurrence and associated pressure pulsations, probably leading to detrimental phenomena; structural vibrations, noise, and machine components breakage among others. Therefore, a deep understanding of the transient pressure variation mechanism and influencing parameters, at different flow domains within these machines, would be a first step toward finding a long term solution to the issue at hand. In this respect, the present article presents an unsteady numerical study, investigating the effect of the blade LE hub position on the PAT pressure field characteristics. The 3D turbulent flow through a centrifugal PAT with three different impellers, namely Rh15, Rh20, and Rh25; has been investigated through a CFD commercial code CFX. Through the analysis of the predicted pressure field characteristics along the full PAT flow passage, a clarification on eventual pressure field characteristics evolution and the influence of impeller outlet design on the same has been made.

2. Geometric model and numerical method

2.1. Geometric model

The investigated model is a six-bladed single suction centrifugal PAT. Designed through a CAD software CF Turbo; the model is composed of three components, namely a single volute scroll casing, shrouded type impeller, and an outlet pipe, with a specific speed Ns = 38.1 under the Best Efficiency Point (BEP) conditions.

$$N_s = 3.64n\sqrt{Q}/H^{0.75} \quad (1)$$

BEP operational parameters; Head (H), Flow (Q) and impeller rotational speed (n) are 22 m, 63.8 m^3/h, and 2900r/min respectively. Other main geometric parameters of the used PAT model are presented through Table 1. In order to investigate the influence of PAT blade trailing edge (BTE) on the flow and pressure field characteristics, three different impellers designs have been used namely Rh15, Rh20, and Rh25 (See Fig. 1). The three impeller models were realized by keeping the blade shroud tip fixed, while radially moving the blade hub tip from 15 mm through 20 mm to 25 mm away from the rotational axis.

Table 1
PAT geometric design parameters.

Parameter	Symbol	Rh15	Rh20	Rh25
Impeller outlet diameter	D_1 (mm)	84.6	84.6	84.6
Impeller inlet diameter	D_2 (mm)	144	144	144
Impeller hub diameter	D_h (mm)	18.12	18.12	18.12
Blade inlet angle	β_2 (°)	22.5	22.5	22.5
Blade outlet angle	β_1 (°)	40.9	31.2°	26.2
Blade trailing edge Radial hub position	Rh (mm)	15	20	25
Impeller inlet width	b_2 (mm)	15.26	15.26	15.26
Blade wrap angle	Φ (°)	111.9	111.9	111.9
Blade number	Z	6	6	6
Volute tongue width	b_3 (mm)	24.7	24.7	24.7
Volute tongue diameter	D_3 (mm)	162	162	162
Volute inlet pipe diameter	D_4 (mm)	75.9	75.9	75.9

2.2. Numerical method

2.2.1. Turbulence modeling

The flow in pump as turbines or any other fluid machinery is controlled by conservation laws expressed through Reynolds-Averaged Navier Stokes (RANS) equations. This system of equations can be closed using different already developed turbulence models, where the k-ε turbulence model figures among the mostly used models for a wide range of flows with industrial engineering applications, which explains its popularity. Simplicity, quick convergence, and the ability to reasonably predict different types of flows are some of its advantages [53–55]. This model is known to express the turbulent eddy viscosity in terms of turbulent kinetic energy k and its dissipation rate ε as follows:

$$\frac{\partial}{\partial t}(\rho k) + \frac{\partial}{\partial x_i}(\rho k u_i) = \frac{\partial}{\partial x_j}\left[\left(\mu + \frac{\mu t}{\sigma_k}\right)\frac{\partial k}{\partial x_j}\right] + G_k + G_b - \rho\varepsilon - Y_M + S_k \quad (2)$$

$$\frac{\partial}{\partial t}(\rho\varepsilon) + \frac{\partial}{\partial x_i}(\rho k u_i) = \frac{\partial}{\partial x_j}\left[\left(\mu + \frac{\mu_t}{\sigma_\varepsilon}\right)\frac{\partial \varepsilon}{\partial x_j}\right] + C_{1\varepsilon}\frac{\varepsilon}{k}(G_k + C_{3\varepsilon}G_b) - C_{2\varepsilon}\rho\frac{\varepsilon^2}{k} + S_\varepsilon \quad (3)$$

with:

$$\mu_t = \rho C_\mu \frac{k^2}{\varepsilon} \quad (3a)$$

where G_k stands for generation of turbulence kinetic energy due to mean velocity gradients, G_b for the generation of turbulence kinetic energy due to buoyancy, Y_M for contribution of the fluctuating dilatation in compressible turbulence to the overall dissipation rate. $C_{1\varepsilon}$, $C_{2\varepsilon}$, and $C_{3\varepsilon}$ are constants. σ_k and σ_ε are the turbulent Prandtl numbers for k and ε, respectively. S_k and S_ε stand for user-defined source terms. Therefore, in the present study, the here-presented *k-ε* turbulence model is used to the solution of the stated RANS equations defining the dynamic laws of water flow through the investigated PAT model.

2.2.2. Numerical scheme

In order to investigate the developed unsteady flow structures as well as resultant pressure field characteristics within the full flow field of the tested PAT model, unsteady numerical simulations of the turbulent flow under part-load flow conditions ($Q/Q_d = 0.67$) were conducted. For the sake of flow field geometrical complexity reduction, both the impeller front and back water chambers were not considered throughout the whole simulation process. For the grid generation of the whole computational flow domain, ICEM-CFD code was used, where structural hexahedral meshes were generated for the entire domain, with finer meshes on blade surfaces (y^+ less than 50) and volute tongue, leading to accurate and well detailed capture of flow structures and their characteristics at those locations.

The grid number can considerably affect the simulation results;

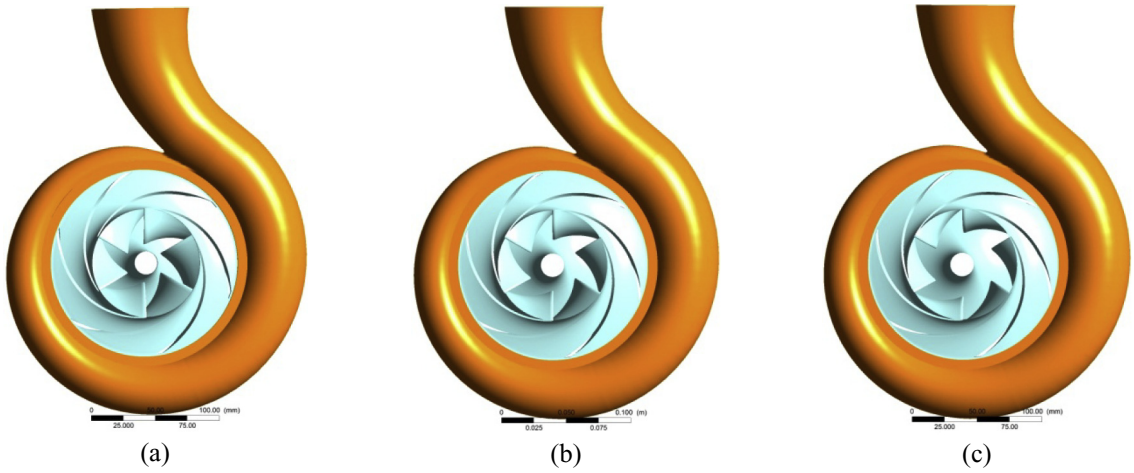

Fig. 1. Three investigated impeller designs: (a) Impeller Rh15, (b) Impeller Rh20, and (c) Impeller Rh25.

therefore it's of a crucial importance to find a number of nodes for which the effect is as negligible possible. In this study, a grid dependence tests was carried out, where the PAT computational domain was meshed with different node numbers (in the range from 700 thousand to 2 million), and steady state numerical simulations were conducted on each set under same operating conditions, to end up with individual developed head values. As it can be seen from Fig. 3(a), the developed head kept on decreasing with the increasing nodes number, where from 1.5 million and beyond the developed head didn't present any remarkable changes. Therefore, in line with the available computational resources, the grid with 1.5 million nodes has been selected as the final grid number for farther simulations. Fig. 2 shows the generated mesh for PAT's three components; namely the volute, impeller and the outlet pipe. Coupled with the Standard k-ε turbulence model, The CFD commercial code ANSYS-CFX is employed to the solution of the Reynolds Averaged Navier-Stokes equations of the 3D unsteady flow through the investigated PAT models. During the simulation process; for a quick solution convergence attainment, steady state simulation was first conducted, the results of which served the initial conditions of the followed transient flow simulations. The boundary conditions, Static pressure (P) and mass flow rate (Q) were respectively imposed at the inlet and outlet locations of the calculated flow domain. For all solid walls, the scalable wall condition was applied, where general connection and frozen-rotor interface types were placed between stationary-stationary and stationary-rotating components respectively. For the case of transient flow simulation, the Transient rotor-stator was applied. Second order accuracy was used for all spatial and temporal derivatives. The time-step for transient simulations was set to 1.14×10^{-4}s, corresponding to 2° of the impeller rotational angle. The convergence criterion was 10^{-6} for all residuals. The selected

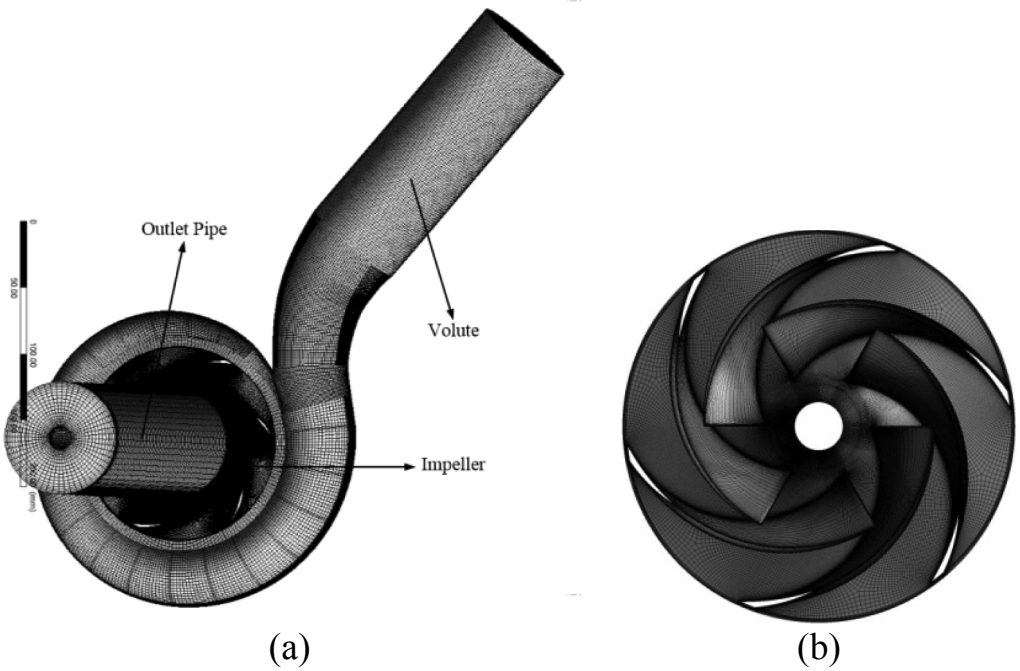

Fig. 2. (a) Mesh assembly for the whole PAT model and (b) generated hexahedral mesh for the impeller.

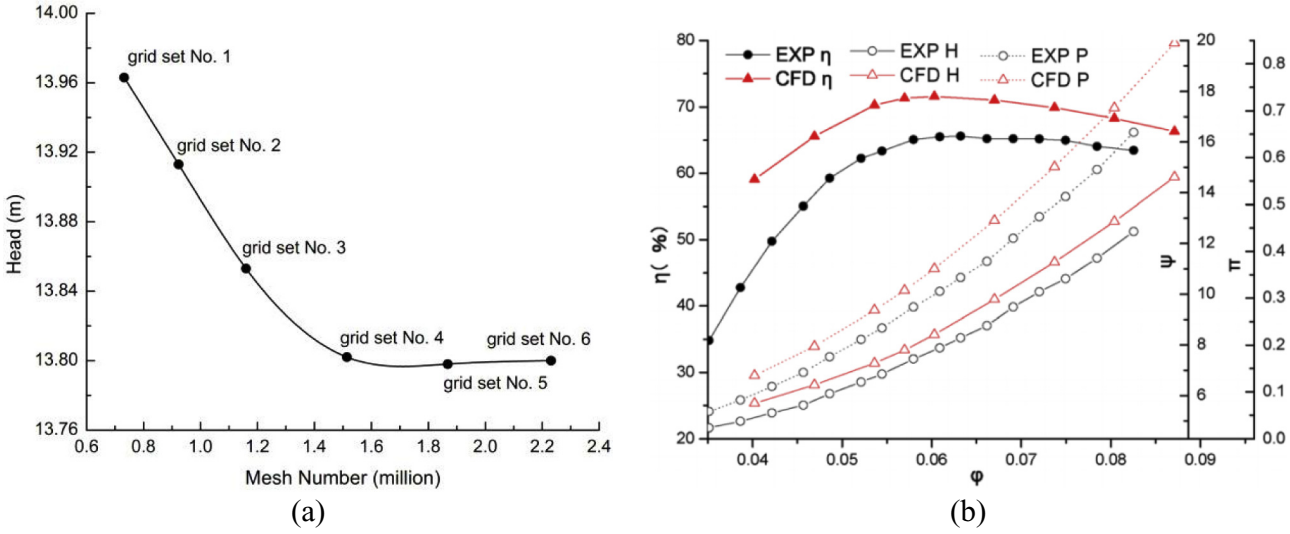

Fig. 3. (a) Mesh independence test in terms of developed head and (b) PAT performance characteristics comparison between experimental and numerical results [35].

fluid was the water at 25 °C. The wall surface roughness was set to 50 μm. In order to avoid reversed flow occurrence thus getting a quite stable flow at inlet and outlet boundaries, five times the pipe diameter extensions were performed at both the extremities. 10 impeller revolutions were simulated where for the sake of conducted analysis accuracy, 5 last revolutions were considered for the pressure field analysis within the flow domain into consideration. 24 pressure monitoring points were fixed at different locations throughout the entire flow domain for an eventual recording of pressure pulsations, leading to a detailed pressure field analysis of the studied flow domain.

The validity of the herein used numerical simulation approach in terms of accurate performance characteristics prediction and flow dynamics capturing within centrifugal PATs has been confirmed by different investigators. Among whom, Yang et al. [35,48] using the same numerical scheme as the one in this study, found acceptable discrepancies between numerical and experimental predictions, with less than 18% error on a global scale, as shown in Fig. 3(b). In this figure the used dimensionless flow, head, and power variables are respectively expressed as [35]:

$$\varphi = Q/nD^3 \quad \psi = gH/n^2D^2 \quad \pi = P/\rho n^3 D^5 \tag{4}$$

3. Results and analysis

3.1. Volute

The turbine operating mode of pump turbines has been found more vulnerable to pressure fluctuations than the pumping mode [17,56]. Moreover, Rotor-stator Interactions (RSI) have been blamed to generate higher pressure fluctuations amplitudes than at any other machine flow domains [21].

The flow in Centrifugal PATs however, may presents different features from normal Pump turbines, as a consequence of lack of flow control system. For the present case, the turbulent pressure distribution contours in the PAT volute at instantaneous time (t = 0.206 s), are presented through Fig. 4. It can be clearly seen that the magnitude of pressure continuously decreases from the volute inlet towards the impeller inlet areas, which itself displays the reality of what is expected to happen in centripetal turbines, where with the gradually reducing spiral casing cross-section, the flow velocity increases causing the local pressure to correspondently drop. At runner flow zones, the water-contained hydraulic energy is transferred to PAT rotor and the connected shaft, for farther energy conversion from mechanical to electrical form within the used electrical generators.

The asymmetric feature of pressure distribution in the volute and impeller, takes source from the asymmetric volute geometry. The pressure is more uniform around the volute inlet flow areas, and get disturbed as it approaches the impeller inlet, where the flow at the volute tongue exhibits comparatively higher pressure gradients, for the three investigated models. Moreover the influence of blade tip periodic passage on volute pressure field is obvious, where formed vortices and wakes at pressure and suction sides of the blade inlet edge, generate periodic pressure variations at points located in the volute near the impeller inlet. Therefore a periodic succession of high and low pressure zones at the impeller inlet areas can be noticed where model Rh15 exhibited higher pressure levels than the rest of models. The extent to which the impeller outlet design influences the pressure pulsations within the volute however, can't be clearly depicted, a reality that calls for more deep investigations on pressure pulsation characteristics at different flow locations within the volute, and the vicinities of impeller inlet flow areas. It's worth noting that, pressure field characteristics within the volute casing has been found to depend on the flow rate where the design flow exhibits smoother flow streamlines both within the volute and then at the inter-blade flow areas, with reduced vortical flow structures, thus providing safe and efficient operating conditions [57–59]. For the off-design (part or over-load) conditions however, the angle with which the flow attacks the blade LE changes from optimum to other values, thus playing source to different flow instabilities occurrence and associated pressure pulsations within the volute and inter-blade flow areas. For instance, in case of hydraulic turbines under part load conditions, flow separation at the runner blade LE may occur due to a positive angle of attack. There here-presented case though, is more into investigating the influence of impeller outlet design on PAT pressure field characteristics where only one flow condition is considered (Q/Qd = 0.67). In order to quantitatively investigate the evolution of pressure pulsation characteristics within the PAT volute, and explore the effect of impeller design on it, five pressure monitoring points have been placed at the center of volute flow

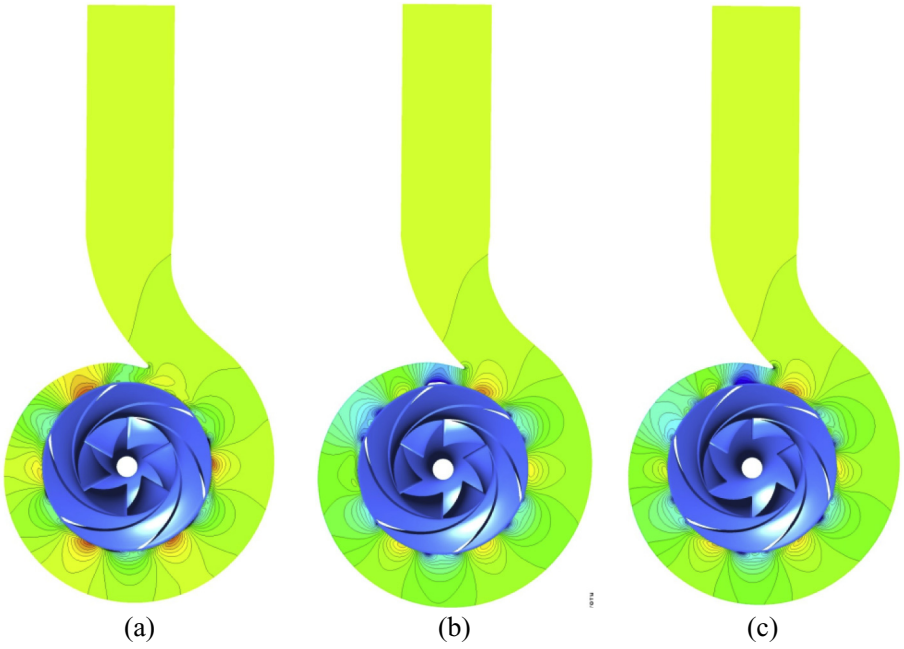

Fig. 4. Unsteady Pressure distribution within the volute (a) Runner with Rh = 15 mm, (b) Runner with Rh = 20 mm, (c) Runner with Rh = 25 mm.

channel as shown in Fig. 5, where the recorded eventual pressure fluctuation data were processed through Fast Fourier Transform (FFT) and the results are presented through Figs. 7 and 8. Fig. 6 presents the time history of pressure pulsations for the four selected points around the impeller for one period time (T = 0.02s) within the three used models. When presenting pressure pulsations characteristics within fluid machinery, it has been a common practice to use their normalized form, which in a certain way ease related analysis [60,61]. Therefore, in this study, pressure pulsations have been normalized to end up with a pressure pulsation coefficient as follows:

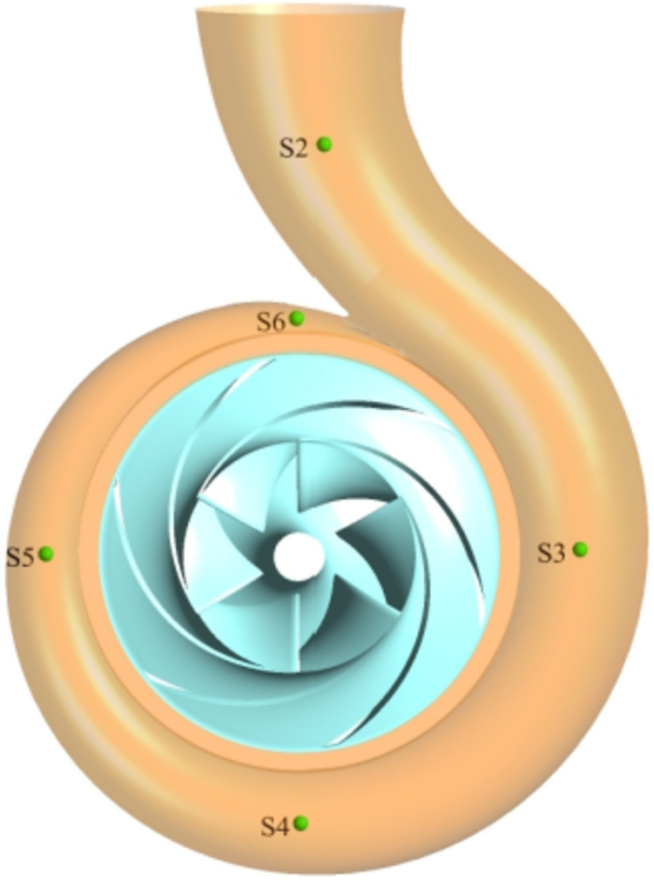

Fig. 5. Pressure monitoring point's positions in the volute flow channel (S2, S3, S4, S5 and S6).

$$Cp = \frac{2P_i}{\rho u_2^2} \tag{5}$$

where P_i and u_2 stand for the individual pressure pulsation amplitude and the tangential speed at the runner inlet, respectively. Being in total agreement with the pressure distribution feature as shown in Fig. 1, the pressure pulsations within the volute at impeller inlet vicinities exhibit an irregular feature where the highest pressure fluctuation amplitudes are recorded with the monitoring point S6 situated somewhere around the volute tongue.

Moreover, from a direct external view, the model Rh20 presented obviously higher amplitude pressure pulsations than the rest of models whereas model Rh15 presented the lowest pressure pulsation amplitudes. Fig. 7 presents a comparative presentation of time domain pressure pulsations at four volute monitoring points for the three impeller blade hub positions (Rh). In the volute, the pressure pulsations at monitoring points S3-S6 have a quite similar trend, where the similarity can be easily noticed at points S4-S6 while S3 presents a complex feature for the three Rh values. This complexity may be taking source from the geometrical position of point S3, being right close to the outlet of the volute inlet pipe outlet, where the water flow, still possessing the high percentage of its momentum, hits the blade pressure side of the blade leading edge, resulting in different complex flow structures formation at the same zones. However, the here presented time domain pressure fluctuations within the volute, only shows the timely pressure variation law, but the influence of impeller outlet design in terms of quantitative figures, is still not very clearly explained. Therefore, a more detailed analysis of volute pressure pulsation frequency spectrum was carried out, where Fast Fourier Transform (FFT) was used to process the recorded pressure data at the same four

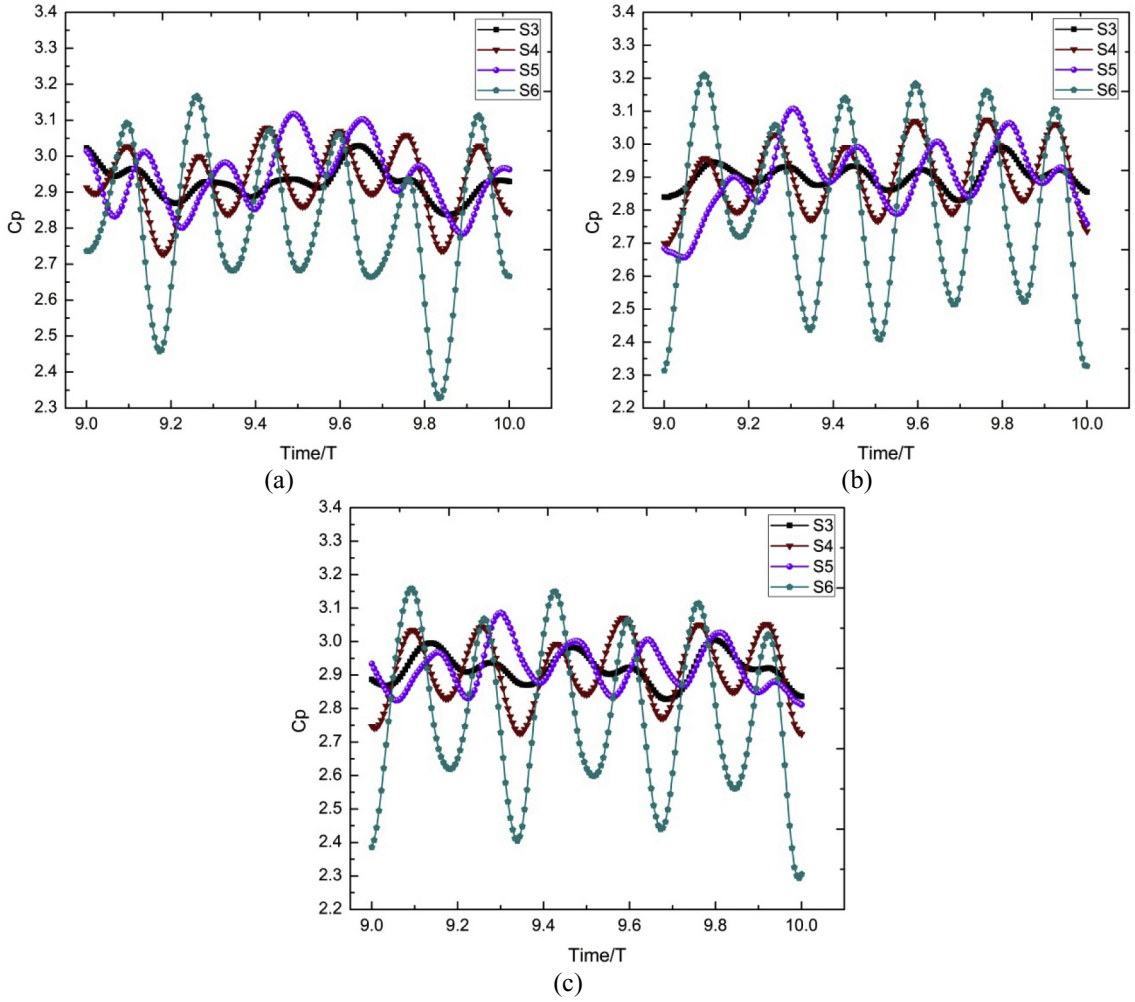

Fig. 6. Time history of pressure variations within the PAT volute for (a) Model Rh15, (b) Model Rh20 and (c) Model Rh25.

monitoring points within volute. Note that for the FFT-based pressure pulsation analysis simplification, individual pressure pulsation amplitudes were normalized by dividing them with $0.5\rho u_2^2$ quantity, as done for simple pressure fluctuation presentation in the above sections.

Fig. 8 shows FFT-based frequency domain pressure pulsations at points S3-S6 for the three investigated Rh values. Note that the impeller rotational speed is 2900 rpm, which indicates that the impeller rotating frequency f_i is 48.3 Hz, leading to the Blade Passing Frequency (f_{BPF}) of 289.8 Hz as the investigated models are six-bladed impellers. The pressure frequency spectrum at Rh25 is the simplest while Rh15 exhibited the complex one with the presence a comparatively higher number of pressure pulsation frequency values, meaning a high level of complex flow movements. The pressure pulsation peak values within the volute are generally found at frequencies integer multiples of the impeller rotating frequency fi; namely twice, three, four, and six times. Such a pressure pulsation is then related to the impeller rotation periodic effect to the volute pressure field. For the three studied Rh values, the blade passing frequency (f_{BPF}) was generally found to be the main frequency, where as shown in Table 2, pressure pulsation amplitudes, at the exception of point S5, continuously increase from point S3 all the way to S6. It can also be noticed that the pressure pulsation amplitude at the main frequency increases from the Rh15 to Rh20, and then drops to Rh25. Therefore, Rh20 volute pressure pulsation was found the highest, whereas Rh15 exhibited the lowest pressure pulsation amplitudes.

3.2. Impeller

Transient pressure distribution within the impeller inter-blade flow zones at the blade mid-span at an instantaneous t = 0.20 s, was shown through Fig. 9 (b). For the three investigated Rh values, owing to the energy transfer between the working fluid medium and impeller blades, the pressure within the impeller inter-blade flow zone generally decreases from the impeller inlet to the outlet, with some flow channels presenting wider lower-pressure zones than others. Higher pressure zones are generally found at every blade's pressure side, right next to blade leading edge (BLE); where, as the flow continues downstream, low pressure zones develop and gradually get wider all the way down to the outlet pipe inlet zone (Impeller outlet).

It can also be noticed that low pressure zone size gradually increased with the Blade Trailing edge hub distance (Rh), leading to Rh25 being the one with biggest low pressure zones at the impeller outlet. The above impeller transient pressure distribution however, can also be explained through the analysis of flow dynamics within the impeller flow field. Fig. 9 (a) shows the flow streamlines within impeller inter-blade flow channels at t = 0.20 s.

As it can be clearly seen, under part-load conditions, transient

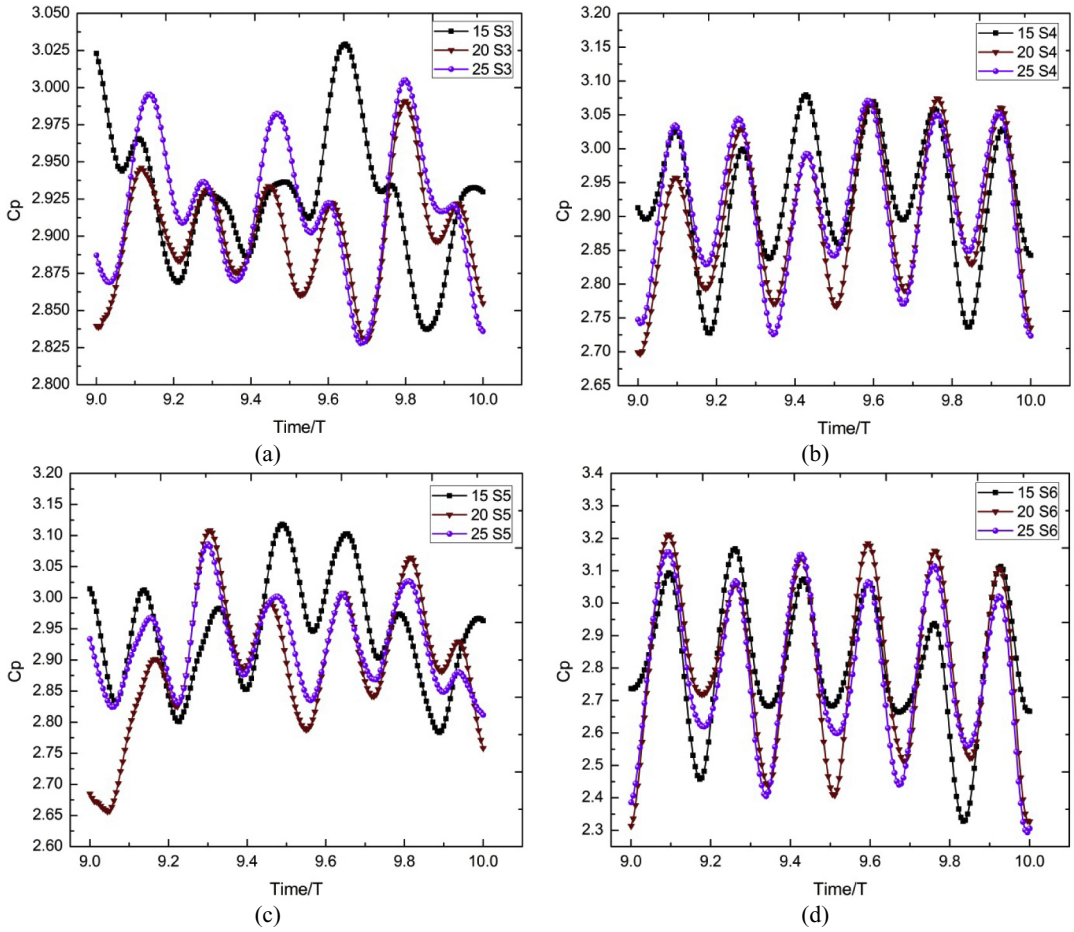

Fig. 7. Time domain of Pressure fluctuations at different monitoring points within the volute: (a) Point S3, (b) Point S4, (c) Point S5, and (d) Point S6.

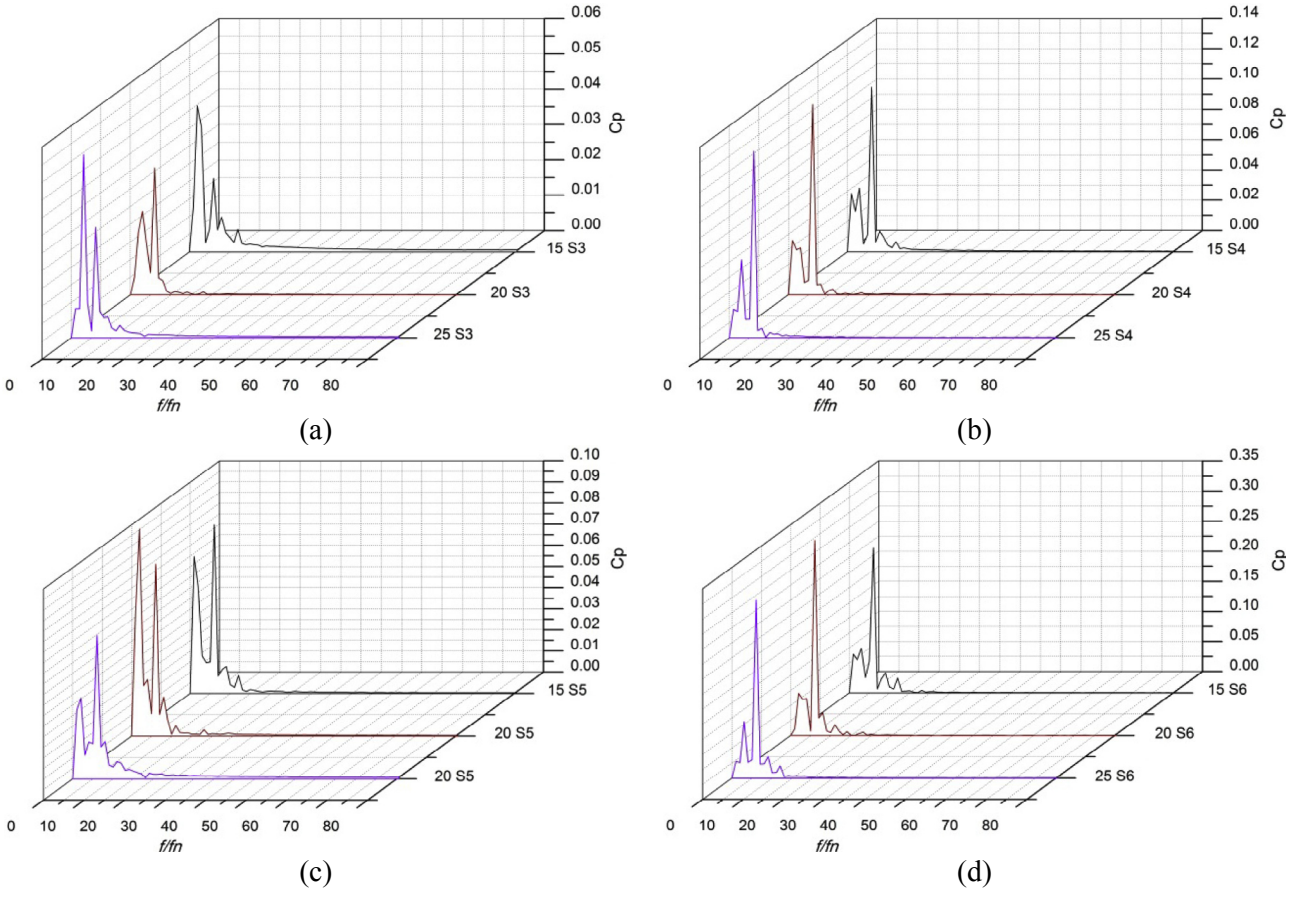

Fig. 8. Frequency domain of Pressure fluctuations at different monitoring points within the volute: (a) Point S3, (b) Point S4, (c) Point S5, and (d) Point S6.

Table 2
Main frequency pressure pulsation amplitudes at different monitoring points within the volute.

Rh (mm)	Main Frequency (Hz)	Amplitudes (Cp)			
		S3	S4	S5	S6
15	6*fi*	0.02080	0.10877	0.07975	0.24092
20	6*fi*	0.03598	0.12548	0.08147	0.32464
25	6*fi*	0.03117	0.12302	0.07629	0.29595

flow separation occurs at the impeller blade LE due to an inadequate flow incidence angle, which in turn generates wakes on the suction side of the impeller blade, partly blocking the inter-blade flow area. The intensity of blade LE wakes is generally a function of the flow incidence angle, which itself depends on many parameters, machine influx and blade inlet angle among others. However, on the present case, none of those is changing, which means that any changes in terms of BLE wake development characteristics may be mainly taking source from the blade trailing edge design modification. Nevertheless, because of the wakes-left out constrained inter-blade flow area, the resultant accelerated inter-blade channel water flow is pushed against the next blade's pressure side, thus creating low static pressure zones on blade pressure side wall. Moreover, because of the velocity gradient between the first blade suction side's wake flow zone and the next blade pressure side's accelerated flow zone, vortex flow development has been observed within some inter-blade flow channels, at the blade trailing edge (BTE)'s upstream zones, mostly attached to the blade suction side. However, because the change of Rh value from 15 mm through 20 mm to 25 mm, which somehow gradually increased the blade camber line radius, hydraulic losses within the impeller inter-blade flow channels have been correspondingly decreasing, which in turn, resulted in a gradual inter-blade flow acceleration and disappearance of the before-noticed blade suction side-attached vortex flow, as Rh increased.

For a more detailed quantitative analysis of pressure pulsation characteristics within the impeller and the influence of impeller outlet design, three pressure monitoring points (I1, I2, and I3) were placed at the center of one inter-blade flow channel as shown in Fig. 10. The time history of pressure variation at three selected monitoring points within the inter-blade flow channel for a two periods time interval are As shown in Fig. 11.

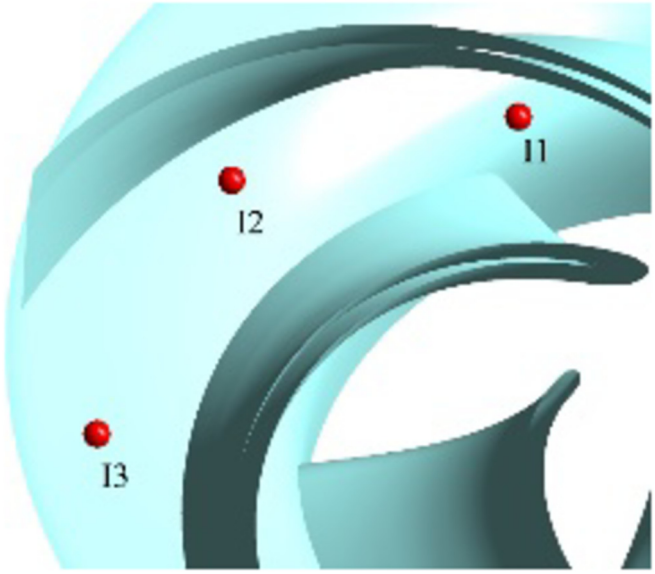

Fig. 10. Pressure monitoring point's positions in the inter-blade flow channel (I1, I2 and I3).

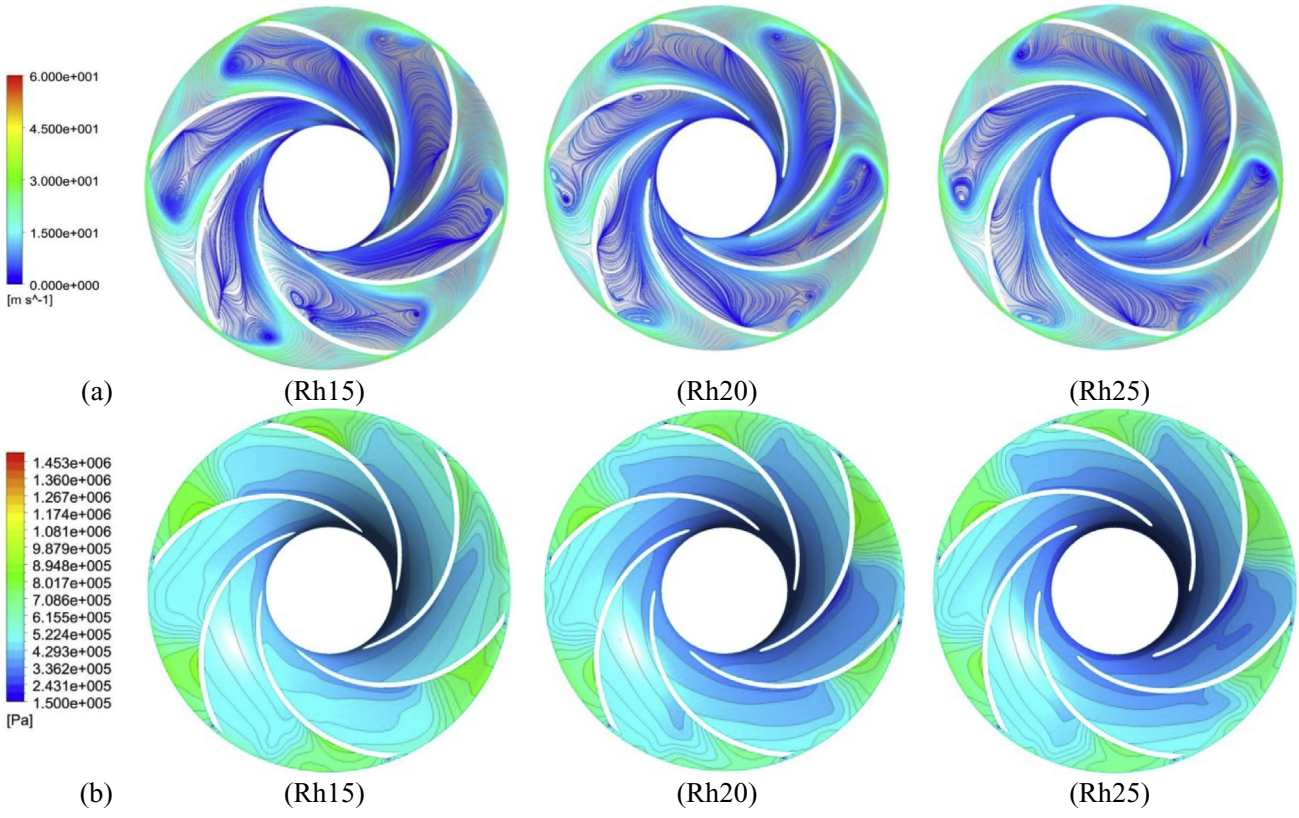

Fig. 9. (a) Impeller mid-span flow streamlines and (b) corresponding pressure distribution contours.

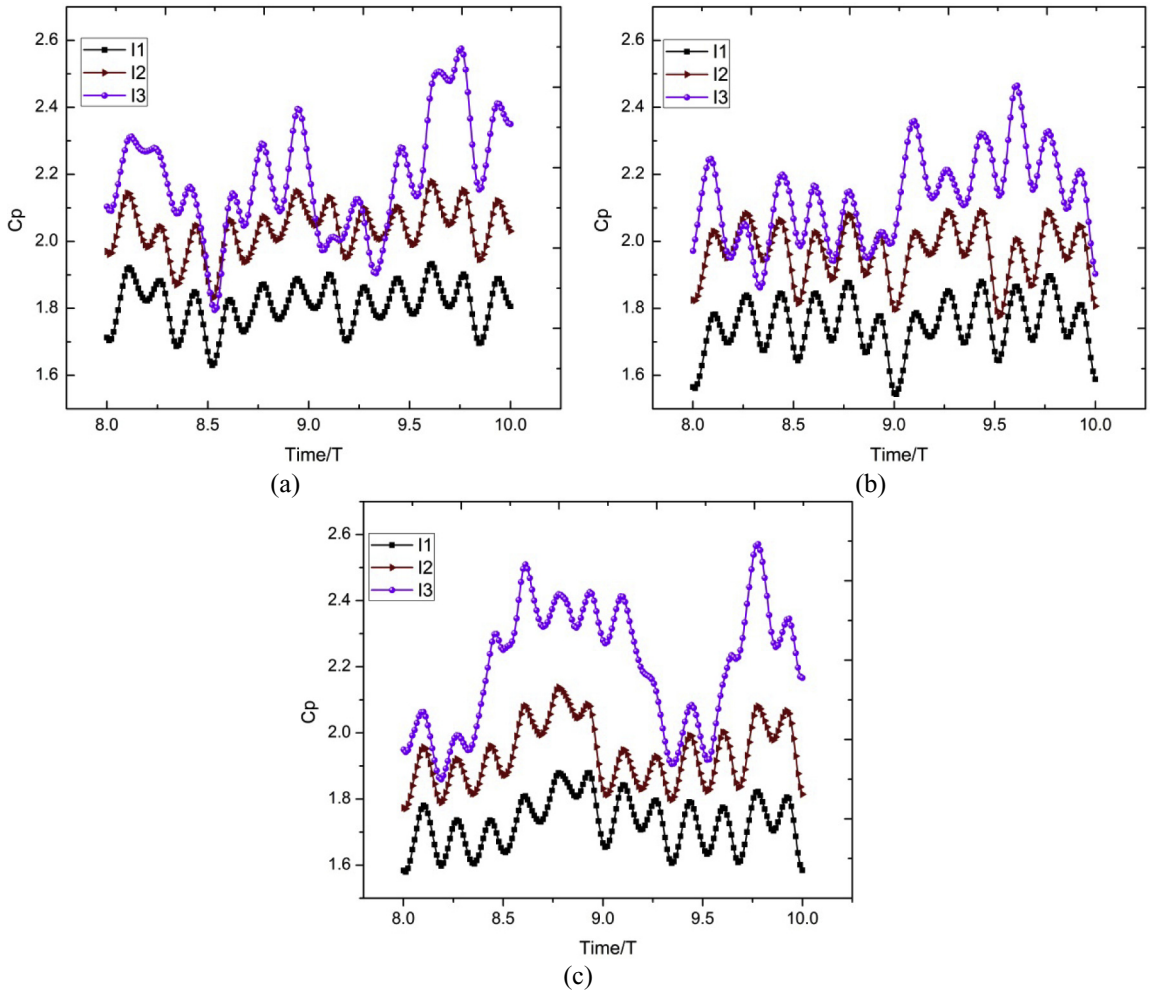

Fig. 11. Time history of pressure variations within the PAT impeller for (a) Model Rh15, (b) Model Rh20 and (c) Model Rh25.

Being in total agreement with Fig. 9(b), the pressure within the impeller gradually decreases from the inlet to the outlet, where, for the three investigated Rh values, pressure pulsation at points I1 and I2 presented an almost same and regular trend; while point I3 located at the impeller inlet's vicinal zones, presented different pressure variation trends for different Rh values. Fig. 12 presents the time domain pressure pulsation for one impeller revolution at the three monitoring points within the impeller flow field. It can be noticed that for points I1 and I2, model Rh15 exhibited higher pressure peaks but with smaller pulsation amplitudes. For point I3, pressure fluctuation rhythm has been different for different Rh values. For a more deep pressure pulsation analysis and BLE design influence, recorded pressure pulsation data at selected monitoring points within the impeller flow field, have been analyzed using Fast Fourier Transform and the results are shown in Fig. 13. Pressure pulsations frequencies within the impeller were found to be dominated by integer multiples of the Blade Passing Frequency (f_{BPF}) from twice to 6 times; and other fractional values such as $f_{BPF}/2$, $f_{BPF}/3$ and so on, which means the presence of many secondary flow structures.

As shown through Table 3, main frequency pressure pulsation amplitudes decreased from the blade LE to the trailing edge for the three studied Rh values. Moreover, main frequency pressure pulsation amplitudes first increased from Rh15 to Rh20 and then dropped to Rh25, making Rh20 the model with highest pressure pulsations and R15 the one with lowest amplitudes.

3.3. Outlet pipe

For a deep pressure field analysis in the outlet pipe flow channel, three equidistant planes: DA at the outlet pipe entrance, DB at 100 mm, and DC at 200 mm downstream have been considered, and five monitoring points have been positioned on each plane, spanning all the radial distance from the shaft to the outlet pipe wall, on each plane as shown in Fig. 14.

Transient Pressure distribution contours at plane DA of each of the three models have been presented through Fig. 15. It can generally be seen that for the three Rh values, pressure increases radially from the center around the shaft to the draft tube walls; and decreases axially from the outlet pipe entrance all along to downstream flow field. This is mainly due to the flow velocity decrease and increase in radial and axial flow directions respectively. The water flow at the impeller outlet exhibits a higher flow tangential velocity component than the radial one, which in turn retards the axial flow movement towards the downstream flow zones. However, as the water gets away from the runner outlet zone, the runner rotational influence on the flow field decreases, which in turn weakens the flow velocity's tangential component, at the same time enhancing the axial one. This gradual increase in the flow axial velocity results in a correspondingly decreasing local pressure as the water travels downstream.

The same truth has been confirmed by the time history of pressure variation in radial and axial direction within the outlet

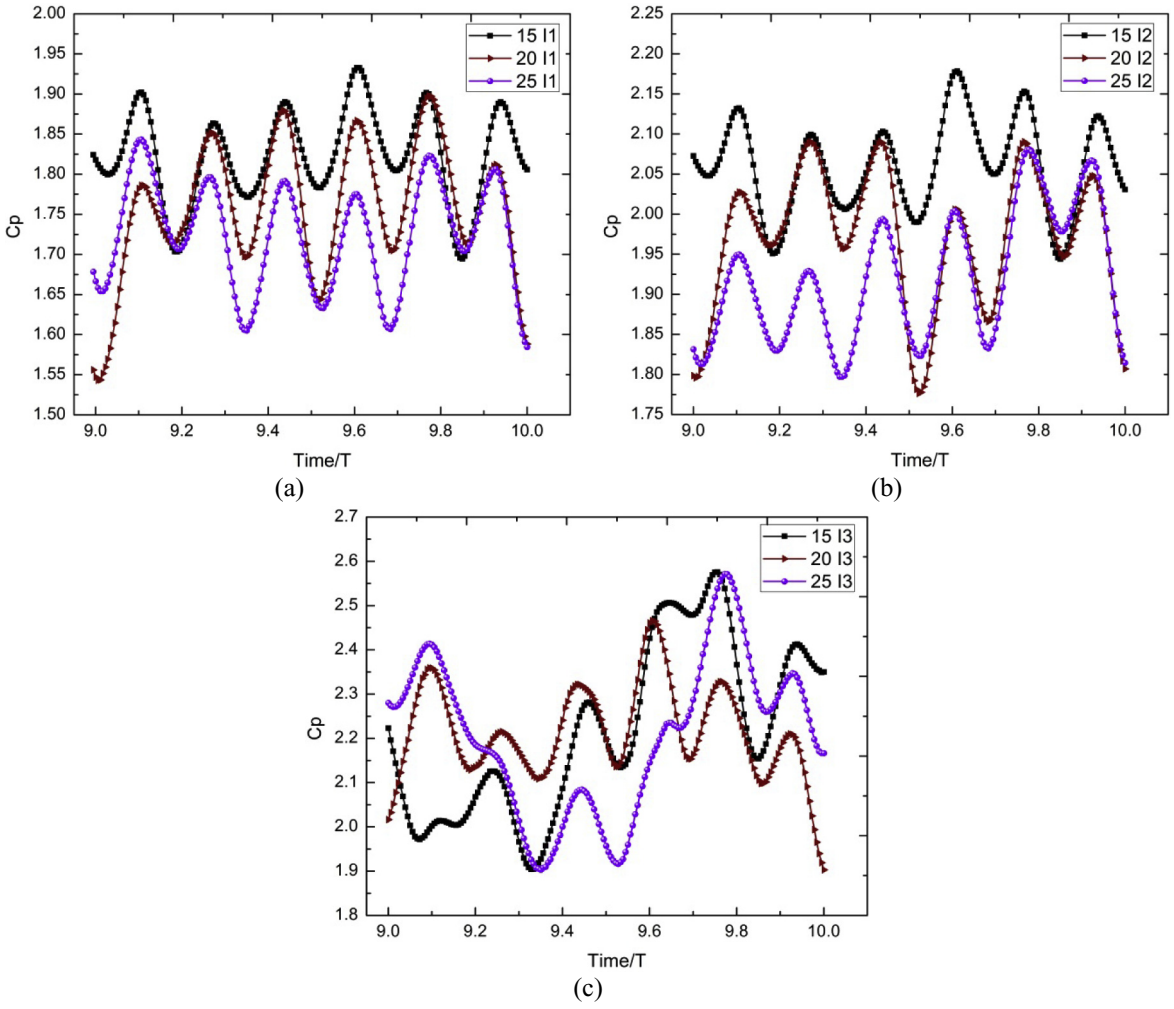

Fig. 12. Time domain of Pressure fluctuations at different monitoring points within the impeller: (a) Point I1, (b) Point I2, and (c) Point I3.

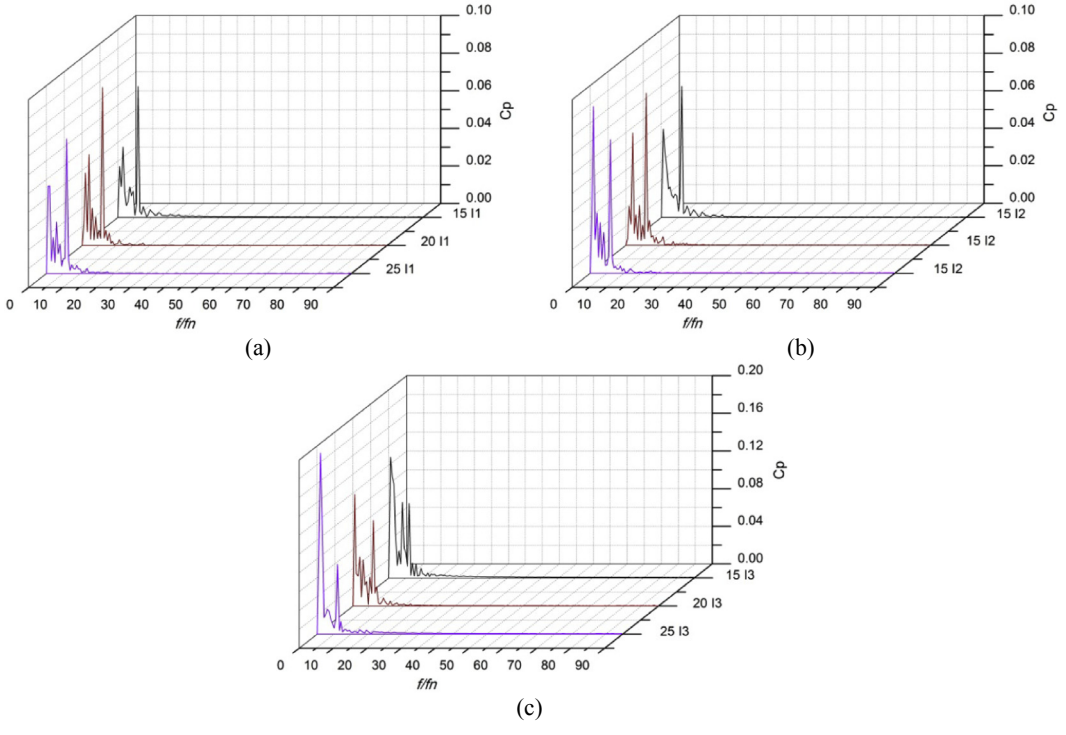

Fig. 13. Frequency domain of Pressure fluctuations at different monitoring points within the Impeller: (a) Point I1, (b) Point I2, and (c) Point I3.

Table 3
Main frequency pressure pulsation amplitudes at different monitoring points within the impeller flow field.

Rh (mm)	Main Frequency (Hz)	Amplitudes (Cp)		
		I1	I2	I3
15	6*fi*	0.06963	0.6981	0.07914
20	6*fi*	0.08091	0.08413	0.09055
25	6*fi*	0.07123	0.07160	0.07409

pipe for Rh15, as presented in Fig. 16. In this figure, pressure fluctuations in both radial (DA1 to DA5) and axial directions (DA1, DB1, and DC1) for one impeller revolution are presented. Speaking of the influence impeller outlet design on pressure pulsations in the outlet pipe, the pressure at the outlet pipe entrance has been generally found to decrease from Rh15 through Rh20 to Rh25; where for Rh15, the influence of blade closeness to the pressure field around the outlet pipe entrance is the most remarkable. The increase in Rh value, affects the runner outlet flow velocity as even shown in Fig. 9.

As the blade trailing edge gets away for the runner rotational axis, the flow velocity's tangential component weakens, giving rise to the axial one. This resulted in a gradually increasing flow velocity, and the corresponding local pressure drop within the outlet pipe flow zones. Both the discussed upstream rotor-stator

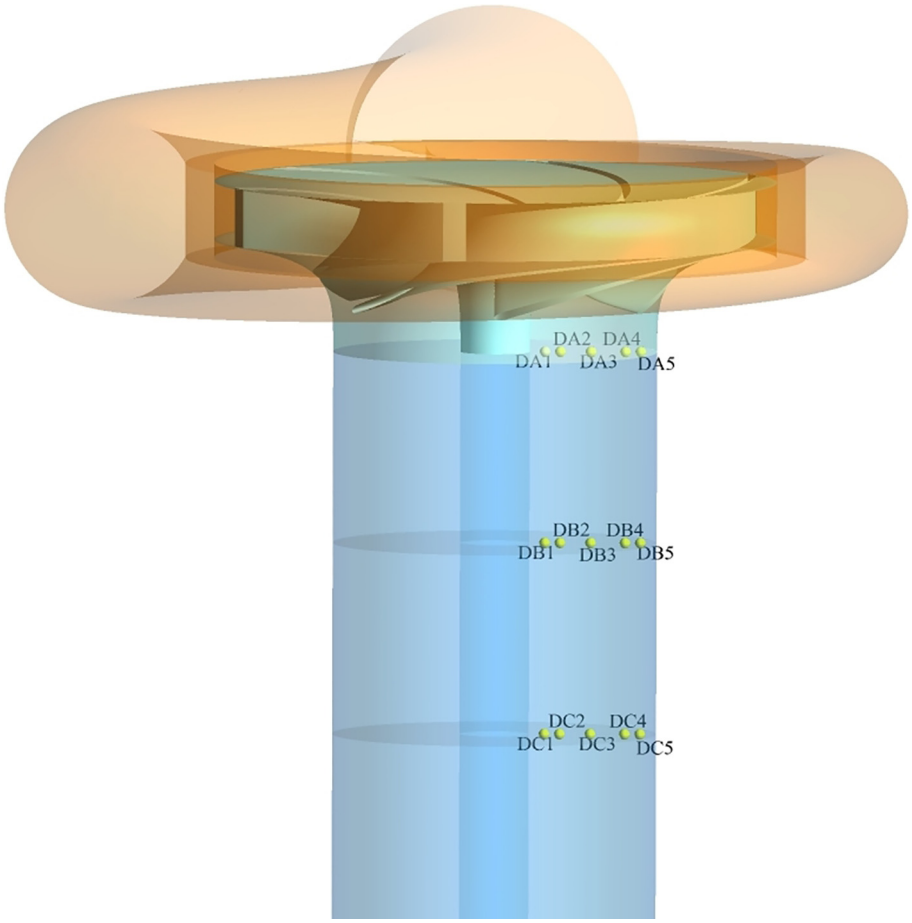

Fig. 14. Pressure monitoring points' positions in the volute flow channel (DA, DB, and DC planes).

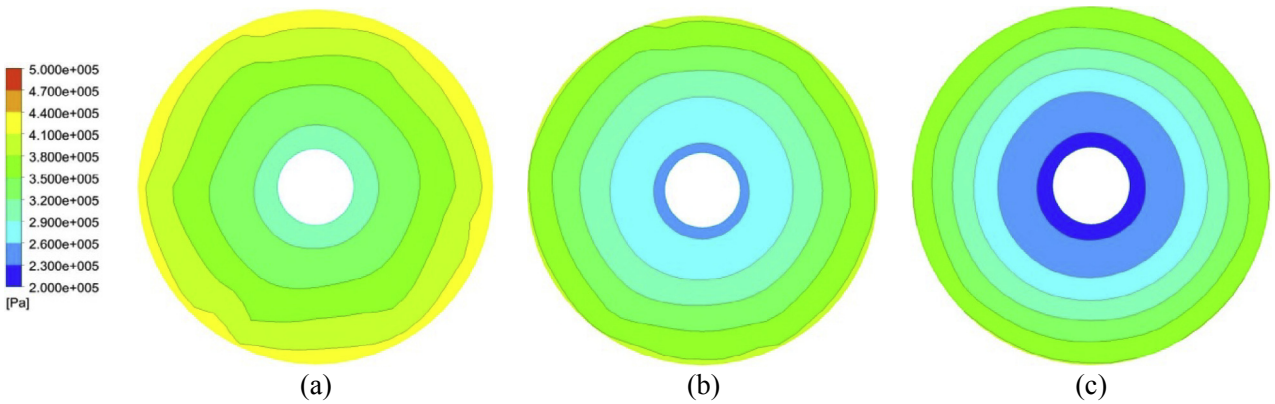

Fig. 15. Pressure distribution contours at the inlet of the outlet pipe at t = 0.020 s: (a) Rh15, (b) RH20, and (c) Rh25.

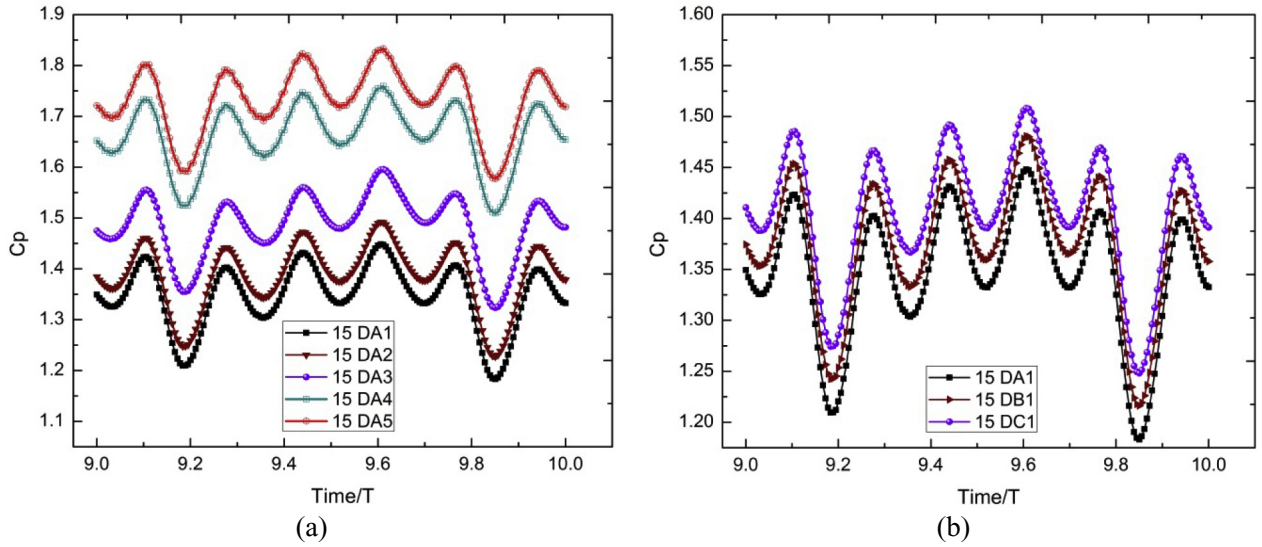

Fig. 16. Time history of pressure distribution within the PAT outlet pipe for (a) Model IA's plane DA, and (b) three inner points on planes DA, DB and DC.

interaction (RSI) and blade closeness to the outlet pipe's inlet zone somehow influenced the turbulent flow characteristics in the outlet pipe and the pressure field characteristics at the same zone.

For a more quantitative pressure pulsation analysis, three pressure monitoring points on the three investigated planes; namely DA1, DB3, and DC5; have been selected for the analysis of impeller outlet design influence on pressure pulsations within the outlet pipe. Fig. 17 shows the time domain pressure pulsation at selected

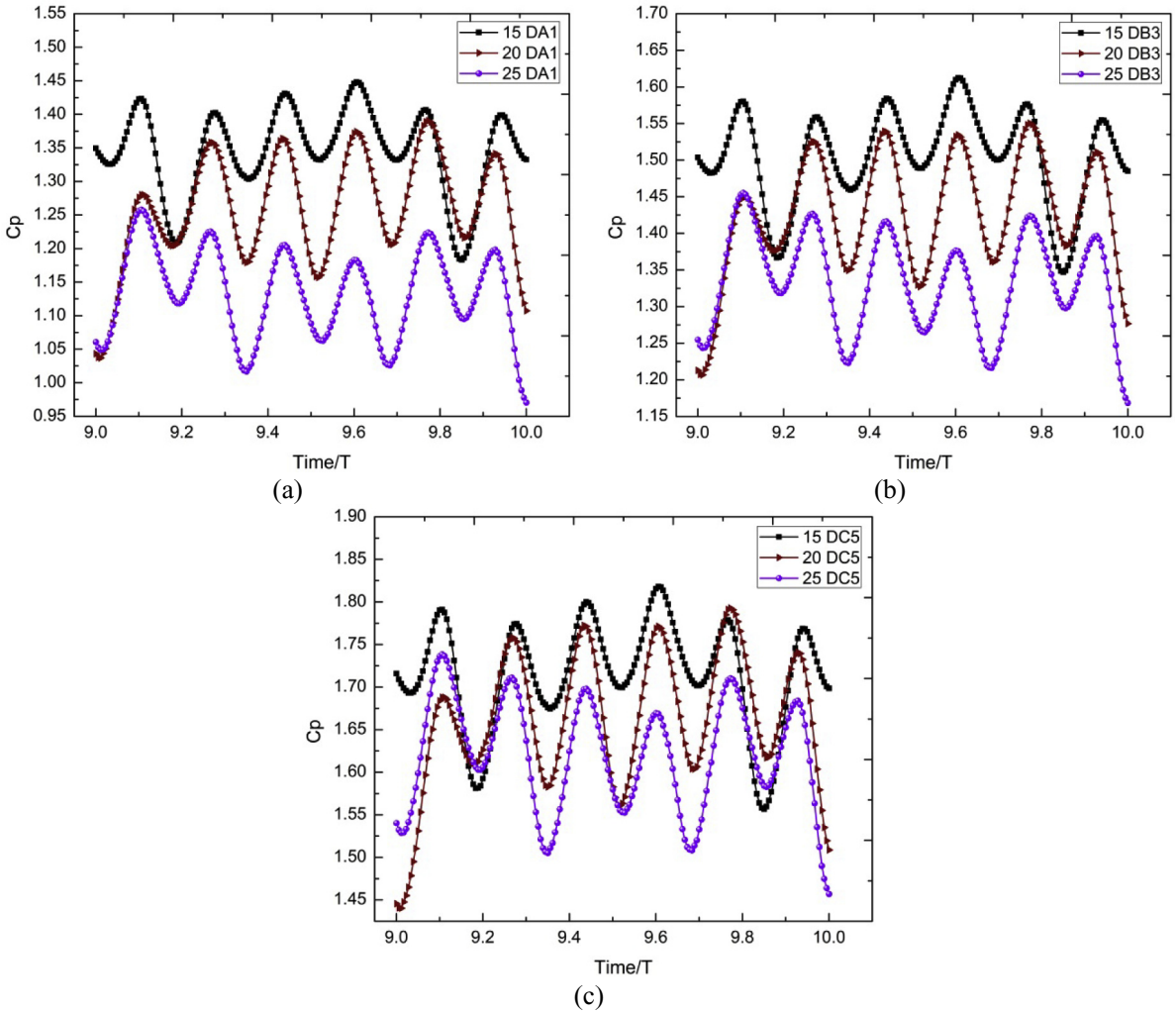

Fig. 17. Time domain of Pressure fluctuations at different monitoring points within the outlet pipe: (a) Point DA1, (b) Point DB3, and (c) Point DC5.

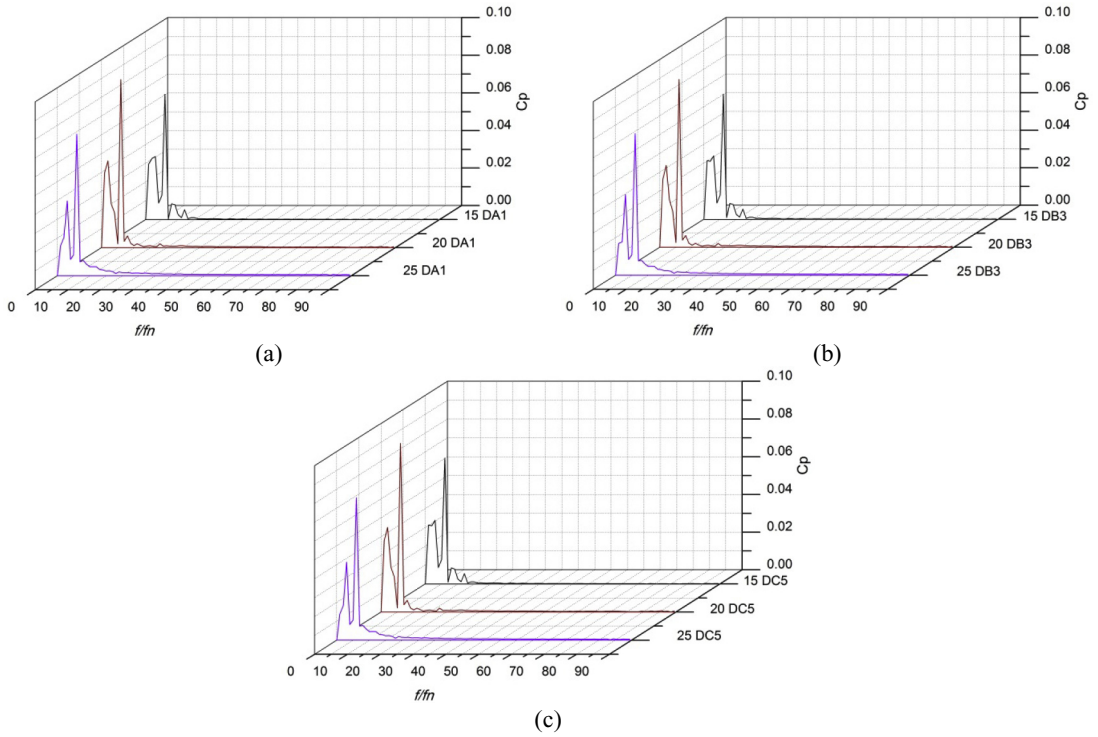

Fig. 18. Frequency domain of Pressure fluctuations at different monitoring points within the outlet pipe: (a) Point DA1, (b) Point DB3, and (c) Point DC5.

Table 4
Main frequency pressure pulsation amplitudes at different monitoring points within the outlet pipe flow channel.

Rh (mm)	Main Frequency (Hz)	Amplitude (Cp)		
		DA1	DB3	DC5
15	6*fi*	0.06676	0.06667	0.066672
20	6*fi*	0.08945	0.08937	0.08938
25	6*fi*	0.07527	0.07546	0.075475

monitoring points for the three Rh values. The similarity of pressure variation trend for all the investigated points is obvious, where Rh15 and Rh25, in good agreement with Fig. 15, exhibited highest and lowest pressure values respectively, at each of the three investigated points. However, this is just about local pressure levels, which is different from pressure pulsation frequency and amplitudes.

Fig. 18 presents the FFT-based frequency domain pressure pulsations at the monitoring points for the three Rh values. The peak pressure pulsation amplitudes have been mainly found to appear at frequencies integer multiples of *fi*, where Rh15 exhibited a wider range of pressure pulsation frequencies with comparatively low amplitudes. The blade passing frequency (f_{BPF}) was found to be the main frequency for the three investigated Rh values, and as shown through Table 4, Rh 20 exhibited the highest main frequency pressure pulsation amplitudes, while Rh15 exhibited the lowest.

4. Conclusion

In this study, the influence of the impeller outlet design on pressure fluctuation within PAT flow field, was systematically investigated by monitoring pressure pulsations within different PAT components; namely the volute, impeller and the outlet pipe; for three different impeller designs. The investigated impellers differ in the blade trailing edge position from the impeller rotational axis, counted on hub side (Rh); namely 15 mm, 20 mm, and 25 mm. Based on results analysis from the carried out transient numerical simulation of PAT complete flow passage, a number of conclusions have been drawn as follows:

a) The PAT flow structures constitute a potential parameter on which incurred pressure pulsation characteristics prediction can be counted. In this study, runner inlet zone flow separations affected the pressure pulsation characteristics at the same zones. In the same respect, the performed impeller blade design modification led to different flow structures development modes, which in turn resulted in different pressure pulsation characteristics.
b) For the three investigated Rh values, at different monitoring points within the whole PAT flow field, pressure pulsation main frequencies have been found to generally be the impeller rotational frequency and its multiples. However, more low frequency components associated with local flow instabilities have also been recorded. The rotor-stator interaction (RSI) therefore, constitutes the main factor greatly influencing PAT pressure pulsations characteristics, where the Blade Passing Frequency (BPF) has been found to be the main frequency within the three PAT components (volute, impeller and outlet pipe).
c) Among the three investigated PAT models, the model with blade trailing edge hub distance of 20 mm (Rh20) exhibited highest pressure pulsations while the one with Rh:15 mm presented the lowest level of pressure pulsations. Therefore, there have not been found a regular rule of pressure pulsation variation with the changing blade trailing edge position.

Acknowledgement

This work is supported by National Natural Science Foundation of China (51506037, 51276046, 71390522), Foundation for Innovative Research Groups of the National Natural Science Foundation of China (51421063), and the Fundamental Research Funds for the Central Universities (HIT.NSRIF.2017047).

References

[1] T. Chen, Y. Zhang, S. Li, Instability of large-scale prototype Francis turbines of Three Gorges power station at part load, Proc. Inst. Mech. Eng. Part A J. Power Energy 230 (7) (2016) 619–632.
[2] M. Binama, et al., Investigation on pump as turbine (PAT) technical aspects for micro hydropower schemes: a state-of-the-art review, Renew. Sustain. Energy Rev. 79 (2017) 148–179.
[3] Y. Zhang, et al., A review of methods for vortex identification in hydroturbines, Renew. Sustain. Energy Rev. 81 (2018) 1269–1285.
[4] Y. Zhang, et al., A review of microscopic interactions between cavitation bubbles and particles in silt-laden flow, Renew. Sustain. Energy Rev. 56 (2016) 303–318.
[5] J. Li, Y. Zhang, J. Yu, Experimental investigations of a prototype reversible pump turbine in generating mode with water head variations, Sci. China Technol. Sci. 61 (4) (2018) 604–611.
[6] J.l. Yin, et al., A hybrid energy storage system using pump compressed air and micro-hydro turbine, Renew. Energy 65 (2014) 117–122.
[7] K.S. Balkhair, K.U. Rahman, Sustainable and economical small-scale and low-head hydropower generation: a promising alternative potential solution for energy generation at local and regional scale, Appl. Energy 188 (2017) 378–391.
[8] S. Barbarelli, et al., Procedure selecting pumps running as turbines in micro hydro plants, Energy Proc. 126 (2017) 549–556.
[9] C.P. Jawahar, P.A. Michael, A review on turbines for micro hydro power plant, Renew. Sustain. Energy Rev. 72 (2017) 882–887.
[10] Y. Zhang, et al., Analysis of the vortices in the inner flow of reversible pump turbine with the new omega vortex identification method, J. Hydrodyn. 30 (3) (2018) 463–469.
[11] J. Yin, et al., Investigation of the unstable flow phenomenon in a pump turbine, Sci. China Phys. Mech. Astron. 57 (6) (2014) 1119–1127.
[12] L. Wang, et al., Numerical investigation on the "S" characteristics of a reduced pump turbine model, Sci. China Technol. Sci. 54 (5) (2011) 1259–1266.
[13] J. Yin, et al., Performance prediction and flow analysis in the vaned distributor of a pump turbine under low flow rate in pump mode, Sci. China Technol. Sci. 53 (12) (2010) 3302–3309.
[14] Y. Zhang, et al., Experimental study on the vibrational performance and its physical origins of a prototype reversible pump turbine in the pumped hydro energy storage power station, Renew. Energy 130 (2019) 667–676.
[15] J.-l. Yin, et al., Hydraulic improvement to eliminate S-shaped curve in pump turbine, J. Fluids Eng. 135 (7) (2013), 071105.
[16] G. Olimstad, T. Nielsen, B. Børresen, Dependency on runner geometry for reversible-pump turbine characteristics in turbine mode of operation, J. Fluids Eng. 134 (12) (2012) 121102.
[17] B. Zhu, et al., Investigation on flow characteristics of pump-turbine runners with large blade lean, J. Fluids Eng. 140 (3) (2017) 031101–031101-9, https://doi.org/10.1115/1.4037787. ISSN: 0098-2202.
[18] R. Tao, et al., Improving the cavitation inception performance of a reversible pump-turbine in pump mode by blade profile redesign: design concept, method and applications, Renew. Energy 133 (2019) 325–342.
[19] P. Kerschberger, A. Gehrer, Hydraulic development of high specific-speed Pump-turbines by means of an inverse design method, numerical flow-simulation (CFD) and model testing, in: IOP Conference Series: Earth and Environmental Science, IOP Publishing, 2010.
[20] Y. Zhang, Y. Zhang, Y. Wu, A review of rotating stall in reversible pump turbine, Proc. Inst. Mech. Eng. Part C J. Mech. Eng. Sci. 231 (7) (2017) 1181–1204.
[21] Z. Zuo, et al., Pressure fluctuations in the vaneless space of High-head pump-turbines—a review, Renew. Sustain. Energy Rev. 41 (2015) 965–974.
[22] Z. Zuo, et al., S-shaped characteristics on the performance curves of pump-turbines in turbine mode—A review, Renew. Sustain. Energy Rev. 60 (2016) 836–851.
[23] X. Luo, et al., Impeller inlet geometry effect on performance improvement for centrifugal pumps, J. Mech. Sci. Technol. 22 (10) (2008) 1971–1976.
[24] J. Lu, et al., Numerical and experimental investigation on the development of cavitation in a centrifugal pump, Proc. Inst. Mech. Eng. Part E J. Process Mech. Eng. 230 (3) (2016) 171–182.
[25] Y. Liu, et al., Energy performance and flow patterns of a mixed-flow pump with different tip clearance sizes, Energies 10 (2) (2017) 191.
[26] Y. Liu, L. Tan, Tip clearance on pressure fluctuation intensity and vortex characteristic of a mixed flow pump as turbine at pump mode, Renew. Energy 129 (2018) 606–615.
[27] Y. Hao, L. Tan, Symmetrical and unsymmetrical tip clearances on cavitation performance and radial force of a mixed flow pump as turbine at pump mode, Renew. Energy 127 (2018) 368–376.
[28] M.H. Shojaeefard, et al., Numerical study of the effects of some geometric characteristics of a centrifugal pump impeller that pumps a viscous fluid, Comput. Fluids 60 (2012) 61–70.
[29] L. Yabin, et al., Influence of prewhirl angle and axial distance on energy performance and pressure fluctuation for a centrifugal pump with inlet guide vanes, Energies 10 (5) (2017) 1–14 (19961073).
[30] R. Barrio, et al., The effect of impeller cutback on the fluid-dynamic pulsations and load at the blade-passing frequency in a centrifugal pump, J. Fluids Eng. 130 (11) (2008), p. 111102-111102-11.
[31] H. Bing, et al., Effects of meridional flow passage shape on hydraulic performance of mixed-flow pump impellers, Chin. J. Mech. Eng. 26 (3) (2013) 469–475.
[32] J. Pei, et al., Optimization on the impeller of a low-specific-speed centrifugal pump for hydraulic performance improvement, Chin. J. Mech. Eng. 29 (5) (2016) 992–1002.
[33] J. Pei, W. Wang, S. Yuan, Multi-point optimization on meridional shape of a centrifugal pump impeller for performance improvement, J. Mech. Sci. Technol. 30 (11) (2016) 4949–4960.
[34] J.-M. Chapallaz, P. Eichenberger, G. Fischer, Manual on Pumps Used as Turbines, Vieweg, 1992.
[35] S.-S. Yang, et al., Effects of blade wrap angle influencing a pump as turbine, J. Fluids Eng. 134 (6) (2012), p. 061102-061102-8.
[36] S. Rawal, J. Kshirsagar, Numerical simulation on a pump operating in a turbine mode, in: Proceedings of the 23rd International Pump Users Symposium, Texas A&M University, 2007.
[37] R. Lueneburg, R. Nelson, Hydraulic Power Recovery Turbines. Centrifugal Pumps—design and Application, second ed., Gulf Publishing Company, 1992, pp. 246–282.
[38] A. Doshi, S. Channiwala, P. Singh, Inlet impeller rounding in pumps as turbines: an experimental study to investigate the relative effects of blade and shroud rounding, Exp. Therm. Fluid Sci. 82 (2017) 333–348.
[39] P. Singh, F. Nestmann, Internal hydraulic analysis of impeller rounding in centrifugal pumps as turbines, Exp. Therm. Fluid Sci. 35 (1) (2011) 121–134.
[40] B. Gao, et al., Influence of the blade trailing edge profile on the performance and unsteady pressure pulsations in a low specific speed centrifugal pump, J. Fluids Eng. 138 (5) (2016), p. 051106-051106-10.
[41] T. Wang, et al., The method for determining blade inlet angle of special impeller using in turbine mode of centrifugal pump as turbine, Renew. Energy 109 (2017) 518–528.
[42] Y. Sun-Sheng, et al., Numerical research on effects of splitter blades to the influence of pump as turbine, Int. J. Rotating Mach. 2012 (2012).
[43] R. Barrio, et al., Performance prediction of a centrifugal pump working in direct and reverse mode using computational fluid dynamics, in: International Conference on Renewable Energies and Power Quality, Granada, Spain, 2010.
[44] S.-S. Yang, et al., Effects of the radial gap between impeller tips and volute tongue influencing the performance and pressure pulsations of pump as turbine, J. Fluids Eng. 136 (5) (2014), 054501.
[45] S. Derakhshan, N. Kasaeian, Optimization, numerical, and experimental study of a propeller pump as turbine, J. Energy Resour. Technol. 136 (1) (2014), 012005.
[46] S.-S. Yang, et al., Effects of impeller trimming influencing pump as turbine, Comput. Fluids 67 (2012) 72–78.
[47] S.-S. Yang, et al., Experimental, numerical, and theoretical research on impeller diameter influencing centrifugal pump-as-turbine, J. Energy Eng. 139 (4) (2013) 299–307.
[48] S.-S. Yang, et al., Research on blade thickness influencing pump as turbine, Adv. Mech. Eng. 6 (2014) 190530.
[49] S.-S. Yang, et al., Influence of blade number on the performance and pressure pulsations in a pump used as a turbine, J. Fluids Eng. 134 (12) (2012) 124503.
[50] S.-S. Yang, S. Derakhshan, F.-Y. Kong, Theoretical, numerical and experimental prediction of pump as turbine performance, Renew. Energy 48 (2012) 507–513.
[51] S. Huang, et al., Performance prediction of a centrifugal pump as turbine using rotor-volute matching principle, Renew. Energy 108 (2017) 64–71.
[52] M. Rossi, M. Renzi, A general methodology for performance prediction of pumps-as-turbines using artificial neural networks, Renew. Energy 128 (2018) 265–274.
[53] M. Woelke, Eddy Viscosity Turbulence Models Employed by Computational Fluid Dynamics, Transaction of the Institute of Aviation, 2007.
[54] H. Versteeg, W. M, An Introduction to Computational Fluid Dynamics: the Finite Volume Method. 2 Ed, Pearson Education Limited, Edinburgh-England, 2007, p. 518.
[55] G.C.-B. Christophe Bailly, in: D.R. Wolfgang Merzkirch, Tropea Cameron (Eds.), Turbulence. Experimental Fluid Mechanics, Springer, Cham, Switzerland, 2015, p. 375.
[56] M. Zangeneh, A compressible three-dimensional design method for radial and mixed flow turbomachinery blades, Int. J. Numer. Methods Fluid. 13 (5) (1991) 599–624.
[57] A.J. Stepanoff, Centrifugal and Axial Flow Pumps: Theory, Design, and Application, Wiley, New York, 1957.
[58] H.W. Iversen, R.E. Rolling, J.J. Carlson, Volute pressure distribution, radial force on the impeller, and volute mixing losses of a radial flow centrifugal pump, J. Eng. Power 82 (2) (1960) 136–143.
[59] K.W. Cheah, T.S. Lee, W. S.H, Numerical study of inlet and impeller flow structures in centrifugal pump at design and off-design points, Int. J. Fluid Mach. Syst. 4 (1) (2011) 25–32.
[60] J.F. Guelich, U. Bolleter, Pressure pulsations in centrifugal pumps, J. Vib. Acoust. 114 (2) (1992) 272–279.
[61] R. Spence, J. Amaral-Teixeira, Investigation into pressure pulsations in a centrifugal pump using numerical methods supported by industrial tests, Comput. Fluids 37 (6) (2008) 690–704.